Supplementary materials and methods:

A total of 45 non-small cell lung cancer (NSCLC) tissue samples were procured from 175 patients at XX. All pathological specimens were confirmed to represent NSCLC by board-certified pathologists, with no prior therapeutic intervention administered to patients before pathological diagnosis. Tissue processing was conducted as follows: 4-μm-thick formalin-fixed paraffin-embedded (FFPE) sections underwent deparaffinization via a graded ethanol series, followed by microwave-assisted antigen retrieval. Upon cooling to ambient temperature, sections were first treated with 0.3% hydrogen peroxide (H_2O_2) for 10 minutes to quench endogenous peroxidase activity, then blocked for non-specific binding using 2% fetal bovine serum (FBS) for 15 minutes. Subsequently, sections were incubated overnight at 4°C with a primary antibody against YWHAZ (1:100 dilution; Abcam, Cambridge, UK). Negative control sections received phosphate-buffered saline (PBS) in place of the primary antibody. After thorough washing, biotinylated anti-mouse immunoglobulin G (IgG) was added as the secondary antibody for 30 minutes, followed by a 30-minute incubation with horseradish peroxidase (HRP)-conjugated streptavidin. Finally, sections were counterstained with hematoxylin, dehydrated through graded alcohols, and mounted.

For YWHAZ expression evaluation, a dual-scoring system was applied: staining intensity was categorized into 0 (negative), 1 (weak), 2 (moderate), or 3 (strong); staining extent was scored as 0 (0%), 1 (1%–23%), 2 (25%–49%), 3 (50%–74%), or 4 (75%–100%). The composite score was calculated by multiplying the intensity score with the extent score. Samples were stratified into low YWHAZ expression (0–4 scores) and high YWHAZ expression (>4 scores) groups.

Antigen staining procedures were performed as follows: sections were deparaffinized and rehydrated, then subjected to antigen retrieval using pH 9 Tris/EDTA buffer (Novocastra, Leica Microsystems, Buffalo Grove, IL, USA) in a PT Link Dako instrument (Dako, Agilent, Santa Clara, CA, USA) at 98°C for 30 minutes. After cooling to room temperature, sections were rinsed with PBS, followed by endogenous peroxidase neutralization with 3% H_2O_2 and Fc receptor blocking using a proprietary protein reagent (Novocastra). Specimens were then incubated with a polyclonal rabbit anti-mouse antibody at room temperature for 1 hour. Immunoreactivity was visualized using a polymer-based detection kit (Novocastra) with AEC (3-amino-9-ethylcarbazole, Dako, Agilent) as the chromogenic substrate. Slides were counterstained with Harris hematoxylin (Diapath), mounted, and analyzed under a Leica DM2000 light microscope (Leica Microsystems). Microphotographs were captured using a Leica DFC320 digital camera (Leica Microsystems), with cell quantification performed as previously described [8].

Supplementary Section 1: Image feature extraction

Whole Tumor Features: The 305 three-dimensional features were extracted from the CT scans of the entire tumor. It contains 150 features (texture features: 62, statistical features: 47, morphological features: 41) mentioned in ref (S1) and 155 additional features (laws features: 125, wavelet features:30). The details are described in Section 2. Following the elimination of features with zero standard deviation, a total of 296 informative features remained for subsequent analysis.

Peritumoral features: A peripheral ring surrounding the primary tumor was created with automated dilation of the tumor boundaries by 5 mm and 10mm on the outside of the tumor boundaries. The identical set of 305 3D imaging features was likewise derived from the peritumoral regions extending 5 mm and 10 mm beyond the tumor boundary. After removing features with standard variance of zero, 281 features and 290 features were left.

Lymph node features: The lymph nodes with a short diameter larger than 1cm located in intrathoracic and extrathoracic sites (LNL) were delineated, and the same set of 305 3D imaging features were extracted from each lymph nodes. The average values of all the lymph nodes were regarded as the lymph node features for this patient. If the patient didn't have lymph nodes, all features were assigned as zero. After removing features with standard variance of zero, 267 features were left.

Totally, 1134 features were generated, and the discretization method was based on fixed-bin-number (FBN) with 128 bins [S2], which was the most commonly used with higher stability. Unity-based normalization was applied to the training features to map them within the [0, 1] interval, and the same normalization parameters (min and max from training data) were used to process the test features.

S1. Zwanenburg, A., et al. The image biomarker standardization initiative: standardized quantitative radiomics for high-throughput image-based phenotyping. Radiology, 2020. 295:328-338.

S2. Wang, Helen Yu Chi, et al. The stability of imaging biomarkers in radiomics: a framework for evaluation. Physics in Medicine & Biology, 2019. 64(16): 165012.

Supplementary Section 2: Laws and wavelet features

Laws features:

To capture diverse texture patterns, laws features employ five one-dimensional filters—E5, S5, R5, W5, and L5—each representing edge, spot, ripple, wave, and low-pass characteristics, respectively. By forming all possible triplet combinations, 125 3D filters were synthesized and applied to the image, and the energy of each output was extracted for feature representation. The specific calculation formula is as follows:

$$Energy = \frac{1}{M \times N \times L} \sum_i^M \sum_j^N \sum_k^L h^2(i,j,k) \quad (1)$$

Where M, N and L represent the dimensions of filtered images, $h(i,j,k)$ represents the filtered image.

Wavelet features

The discrete wavelet transform can iteratively decompose an image (3D) into four components. Each iteration splits the image both horizontally and vertically into low-frequency (L) and high frequency (H) components. Thus, four components are generated: a high-pass/high-pass component consisting of mostly diagonal structure, a H/L component consisting mostly of vertical structures, a L/H component consisting mostly of horizontal structure, and a L/L component representing a smoothed approximation of the original image. In subsequent steps, the decomposition is reapplied to the L/L component obtained from the prior step. In this work, decomposition level of 2 was used, which means 15 blocks were generated for 3D decomposition (C1: L/L/L, C2: H/H/L, C3: H/H/H; C4: L/H/L, C5: L/L/H, C6: H/L/H, C7: H/H/H, C8: L/H/H, C9: H/L/L, C10: H/H/L, C11: L/H/L, C12: L/L/H, C13: H/L/H, C14: H/H/H, C15: L/H/H). For each filtered block, the energy (P1) and entropy (P2) were calculated.

$$Energy = \frac{1}{M \times N \times L} \sum_i^M \sum_j^N \sum_k^L h^2(i,j,k) \quad (2)$$

$$Entropy = \frac{-1}{M \times N \times L} \sum_i^M \sum_j^N \sum_k^L \left(\frac{h^2(i,j,k)}{\text{norm}^2}\right) log\left(\frac{h^2(i,j,k)}{\text{norm}^2}\right) \quad (3)$$

Where M, N and L represent the dimensions of filtered images, $h(i,j,k)$ represents the filtered image.

Supplementary Section 3: Radiomics signature calculation formulas

RS_WT=-0.92×Wavelet P2 L2 C15+0.34×Centre of mass shift+0. 46×Compactness 2-0.78×GLSZM_LZLGLE+0.54

RS_Peri5mm=-0.37×Wavelet P1 L2 C13+0.38×IHQCOD+0.44×GLSZM_ZSNU-0.44×Laws features L5 L5 R5+0.44

RS_Peri10mm= 0.35×Statistical ENERGY-0.27×Wavelet P1 L2 C14-0.21× Statistical Coefficient of variance+0.68

RS_lymph node=-0.70×GLSZM_ZSNUN +0.22×MHG-2.83×LF L5 L5 R5+3.11×LF L5 R5 L5+0.65

RS_WP=5.00 ×RS-WT+3.73 ×RS_Peri5mm-4.67

RS_WPL=6.82 × RS_WT+3.61 × RS_Peri5mm+6.36 × RS_lymphnode-9.18

GLSZM_LZLGLE：GLSZM_Large zone low grey level emphasis

IHQCOD：Intensity histogram quartile coefficient of dispersion

GLSZM_ZSNU： GLSZM_Zone size non-uniformity

GLSZM_ZSNUN: GLSZM_Zone size non-uniformity normalised

MHG: Minimum histogram gradient

LF L5 L5 R5: Laws features L5 L5 R5

LF L5 R5 L5: Laws features L5 R5 L5

Supplemental Table 1 The distributions and comparison of lymph node between DCB and NDB

Lymph node	Training cohort			Test cohort		
	DCB	NDB	*P*	DCB	NDB	*P*
lymph1	34(57.6)	24(52.2)	0.69	20(51.3)	15(48.4)	1
lymph2	35(59.3)	32(69.6)	0.31	15(38.5)	17(54.8)	0.23
lymph3	13(22.0)	9(19.6)	0.81	9(23.1)	3(9.7)	0.2
lymph4	10(16.9)	10(21.7)	0.62	10(25.6)	6(19.4)	0.58
lymph5	27(45.8)	23(50)	0.7	20(51.3)	15(48.4)	1
lymph6	24(40.7)	25(54.3)	0.17	17(43.6)	12(38.7)	0.81
lymph7	16(27.1)	6(13.0)	0.094	9(23.1)	7(22.6)	1
lymph8	26(44.1)	24(52.2)	0.44	17(43.6)	11(35.5)	0.62
lymph9	11(18.6)	7(15.2)	0.8	6(15.4)	5(16.1)	1
lymph10	19(32.2)	15(32.6)	1	12(30.8)	12(38.7)	0.61
lymph11	13(22.0)	12(26.1)	0.65	10(25.6)	7(22.6)	1
lymph12	13(22.0)	10(21.7)	1	7(17.9)	5(16.1)	1
lymph13	7(11.9)	7(15.2)	0.77	5(12.8)	2(6.5)	0.45
lymph14	4(6.8)	2(4.3)	0.69	2(5.1)	1(3.2)	1

Note: The comparison of the number of metastatic lymph node in different locations was Fisher's test. The distributions of the lymph nodes were delineated as follows. Lymph1: hilar (Ipsilateral), lymph 2: subcarinal, lymph 3: upper paratracheal (right), lymph 4: upper paratracheal (left) , lymph 5: Subaortic, lymph 6: para-aortic, lymph 7: Prevascular, lymph 8: lower paratracheal (right), lymph 9: lower paratracheal (right), lymph 10: low cervical, supraclavicular, and sternal notch nodes (Ipsilateral), lymph 11: low cervical, supraclavicular, and sternal notch nodes (Contralateral), lymph 12: hilar (Contralateral), lymph 13: Other intrathoracic lymph nodes, lymph 14: Extrathoracic lymph node

Supplementary Table 2 Baseline patients' characteristics of immunohistochemistry

Characteristics	Patients	Characteristics	Patients
Age		Smoke	
Male	35	Non-smoker	41
Female	10	smoker	4
T stage		KPS	
I	9	70	1
II	12	80	26
III	8	90	17
IV	16	100	1
N stage		PD-L1	
0	3	negative	12
1	2	1-49%	7
2	21	>=50%	9
3	17	unknown	17
M stage		Treatment	
0	14	Monoclonal	10
1a	12	Chemo combined	35
1b	3	Pseudoprogression	4
1c	16	Huperprogression	10
Histology		Histology	
ADC	30	SCC	15
Best response		Clinical benefit	
PD	17	DCB	24
SD	11	NDB	19
PR/CR	17	unknown	2

Supplementary Table 3 Macrophage markers and “complete phenotype” associate with Clinical Benefit

Variables	marker	DCB	NDB	P
TAM	CD68	19.42±13.53	11.71±7.30	0.064
M1 like TAM	CD86	1.16±2.32	1.08±2.62	0.83
M2 like TAM	CD163	16.63±8.98	12.04±7.75	0.045

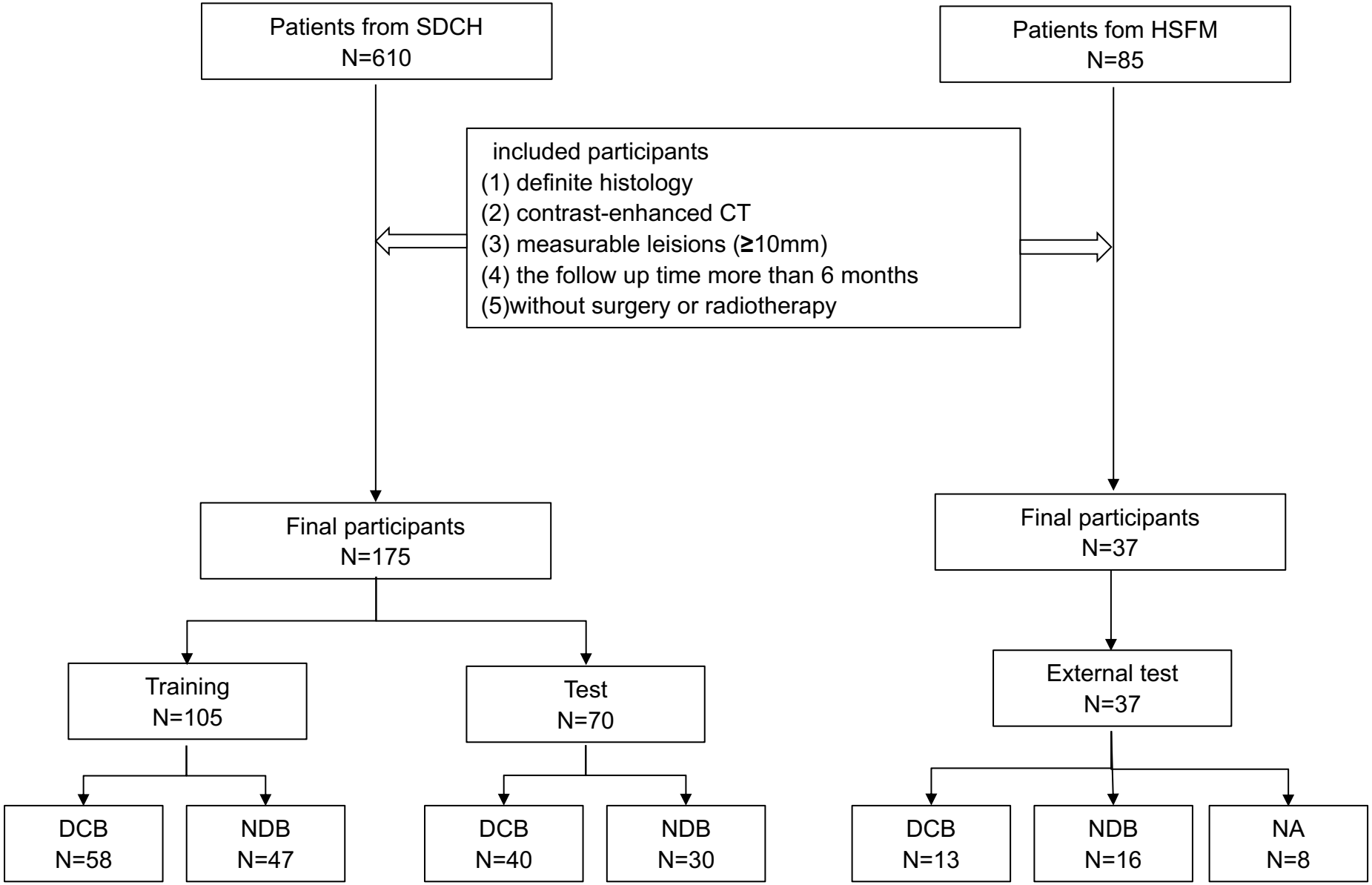
Patients from SDCH
N=610
Patients fom HSFM
N=85
included participants
(1) definite histology
(2) contrast-enhanced CT
(3) measurable leisions (≥10mm)
(4) the follow up time more than 6 months
(5)without surgery or radiotherapy
Final participants
N=175
Final participants
N=37
Training
N=105
Test
N=70
External test
N=37
DCB
N=58
NDB
N=47
DCB
N=40
NDB
N=30
DCB
N=13
NDB
N=16
NA
N=8

Supplementary Figure 1. The flowchart of patient enrollment and grouping

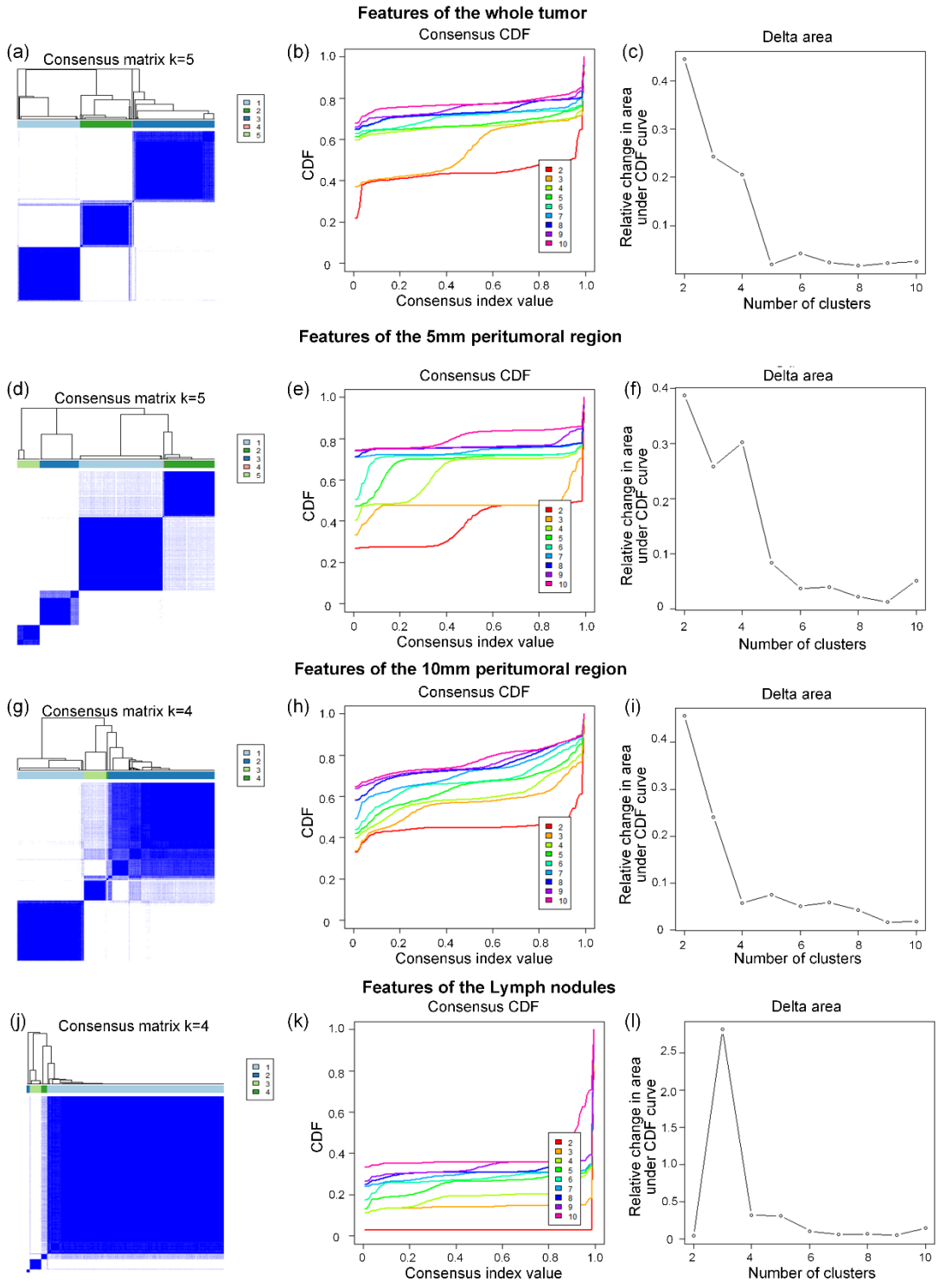

Supplementary Figure 2. Group different radiomic features based on consensus clustering. (a),(d),(g) and (j) The consensus matrix corresponding to the optimal cluster number for features of the whole tumor, 5mm peritumoral region, 10mm peritumoral region and the lymph nodules, respectively.(b), (e), (h) and (k) Consensus empirical cumulative

distribution function (CDF) of all given cluster numbers. (c), (f), (i) and (l) Relative change in area under CDF curves with number of clusters. The range of k change from 2 to 10. The optimal cluster numbers k =5, 5, 4 and 4 were determined by the steepest drop of delta area change.